(will be inserted by the editor)

Directional Frames for Image Recovery: Multi-scale Discrete Gabor Frames

Hui Ji · Zuowei Shen · Yufei Zhao

Received: date / Accepted: date

Abstract Sparsity-driven image recovery methods assume that images of interest can be sparsely approximated under some suitable system. As discontinuities of 2D images often show geometrical regularities along image edges with different orientations, an effective sparsifying system should have high orientation selectivity. There have been enduring efforts on constructing discrete frames and tight frames for improving the orientation selectivity of tensor product real-valued wavelet bases/frames. In this paper, we studied the general theory of discrete Gabor frames for finite signals, and constructed a class of discrete 2D Gabor frames with optimal orientation selectivity for sparse image approximation. Besides high orientation selectivity, the proposed multi-scale discrete 2D Gabor frames also allow us to simultaneously exploit sparsity prior of cartoon image regions in spatial domain and the sparsity prior of textural image regions in local frequency domain. Using a composite sparse image model, we showed the advantages of the proposed discrete Gabor frames over the existing wavelet frames in several image recovery experiments.

Keywords Gabor frames · image recovery

Mathematics Subject Classification (2010) 42C40 · 65T60

1 Introduction

Many types of signals can be sparsely approximated in some transform domain. In recent years, sparse approximation has been an indispensable tool in signal recovery. The success of the sparsity-driven signal recovery methods largely depends on whether the chosen transform can effectively sparsify input signals. For years, real-valued orthogonal *wavelet bases* [12] was prevailing in signal processing as they can effectively model 1D piece-wise smooth signals. Another advantage of orthogonal wavelet bases is that its decomposition process (wavelet transform) and reconstruction process (inverse wavelet transform) are very computationally efficient via the implementation of 1D filter banks. For sparsity-based signal recovery, over-complete systems are usually preferred as they introduce the redundancy helpful to better sparse approximation. Particularly, wavelet tight frames, e.g un-decimal Daubechies wavelet systems [10] and spline framelets [13, 37], are often chosen as the preferred redundant systems, owing to the same fast decomposition and reconstruction processes.

For 2D signals like images, the often used 2D wavelet tight frames (or bases) are generated via the tensor product of two 1D wavelet tight frames (or bases) along the horizontal and vertical axes. One advantage of a tensor product real-valued wavelet tight frame lies in the computational efficiency of the associated decomposition and reconstruction processes, which can be implemented using 1D filters banks along two axes. Such computational efficiency is important to most sparsity-based image recovery methods, since they iterate a back-and-forth process between image domain and frame coefficient domain. The disadvantage of tensor product real-valued wavelet tight frames is that their orientation selectivity is limited to only two directions. Different from 1D piece-wise smooth signals, real images often contain both cartoon parts and texture parts. Cartoon parts show piece-wise smooth content, whose discontinuities (edges) have geometrical regularity along the edge directions. Texture parts are highly non-smooth, but show small elements displaying either random or periodic patterns. Therefore, the design of a good redundant system for sparsity-based image recovery should be able to effective characterize both directional regularity of image edges and texture components with local periodicity and have efficient decomposition and reconstruction processes.

Many real-valued frames or tight frames have been proposed to improve orientation selectivity, including *curvelets* [7], *bandlets* [30], *composite wavelet* [22], *shearlets* [25], among many others. Most of these frames/tight frames

Hui Ji, Zuowei Shen and Yufei Zhao
Department of Mathematics, National University of Singapore, Lower Kent Ridge Road, Singapore 119076
E-mail: matjh,matzuows,a0086274@nus.edu.sg

introduce additional orientations via replacing isotropic scaling matrices used in tensor product 2D wavelets by iso-isotropic scaling matrices. For example, together with parabolic matrices, shearing matrices are used in shearlets and composite wavelets for gaining additional orientations, and rotating matrices are used in curvelets for gaining additional orientations. Despite the improvement on orientation selectivity, the existing implementations of these frame systems are much less efficient than the 1D filter bank based implementation of tensor wavelet tight frames.

Another promising approach to gain orientation selectivity without sacrificing computational efficiency is using complex-valued systems. Different from real-valued functions, the real/imaginary part of the tensor product of two 1D complex-valued functions is not separable by itself. Thus, a 2D complex-valued tensor system can have better orientation selectivity using carefully chosen 1D real and imaginary functions. For wavelet systems, the so-called *dual-tree complex wavelet transform* [39] used two different discrete orthogonal wavelet bases to produce a 2D tensor complex-valued wavelet tight frame whose real part and imaginary part have up to six orientations, which still leaves the room for increasing orientation selectivity. In addition, wavelet systems cannot model well texture regions that display periodic local patterns. For Gabor systems, the local Fourier analysis based systems, e.g. local *discrete cosine transform* (DCT), are introduced in the literature for modeling such regularly textured regions. However, same as real-valued 2D tensor wavelet frames, real-valued 2D local DCT also lacks orientation selectivity which makes it less effective when expressing texture regions with varying oriented periodicity. Complex-valued bi-orthogonal windows Fourier bases are proposed in [31] to do local time-frequency analysis for textured images with strong orientation selectivity. Such bi-orthogonal windows Fourier bases lack some important properties for image recovery, e.g., the system redundancy for artifacts suppression in image recovery, zero DC offset of high-pass filters, and fast implementation of signal decomposition/reconstruction. Also, the combination of both Gabor system and wavelet system, e.g., a wavelet frame and a local DCT was proposed for sparsifying natural images with both cartoon regions and textured regions ([3, 44]).

1.1 Motivation

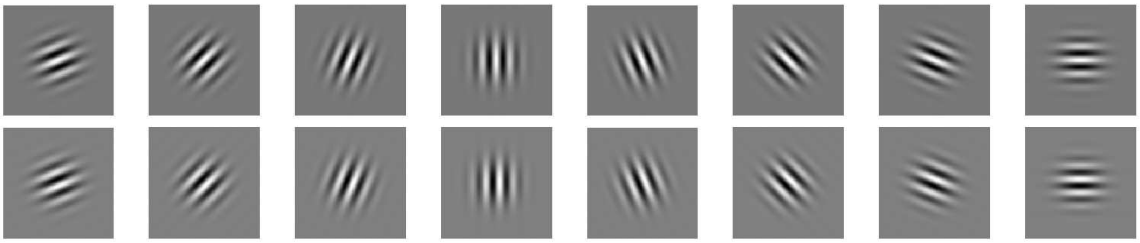

Fig. 1 Illustration of 2D tensor product Gabor functions with different orientations. The real parts of Gabor functions are shown in the top row and the imaginary parts are shown in the bottom row.

In this paper, we are interested in studying discrete frames that are suitable for sparsity-based image recovery with the following three properties: 1) high orientation selectivity; 2) powerful expressiveness for both cartoon regions and texture regions; and 3) fast decomposition and reconstruction processes. The advantage of complex-valued tensor product functions on orientation selectivity leads us to consider Gabor functions $g(x)e^{2\pi i\omega x}$ defined by the modulation of a Gaussian-like window function g . 2D tensor product Gabor functions $g(x_1)g(x_2)e^{2\pi i(\omega_1 x_1+\omega_2 x_2)}$ can provide arbitrary orientation selectivity by choosing different frequency pairs (ω_1, ω_2). In other words, different modulations gives different orientations of 2D Gabor functions; see Fig. 1 for an illustration.

In addition, 2D Gabor functions can effectively model both cartoon regions and texture regions by using the window functions with different supports. In image processing, when using a window function of small support, the imaginary part of a Gabor function (sine function) often is understood as a first-order partial differential operator, and its real part (cosine function) is understood as a second-order partial differential operator. For example, the discrete high-pass filters with support 3×3 in our construction has real part $[-1, 2, 1]$ and imaginary part $[1, 0, -1]$ up to a constant. Thus, it can measure local image gradients of multiple orders for cartoon regions with piece-wise smoothness. For texture regions with sparse local frequencies, the Gabor function with Gaussian-like window functions of sufficiently large support, is well-known for its optimality on local time-frequency analysis by *Heisenberg Uncertainty Principle*.

The advantages of 2D Gabor functions on orientation selectivity and local time-frequency analysis make them a very good tool for image analysis. Daugmann [14] showed that simple cells in the visual cortex of mammalian brains can be modeled by a wavelet system generated by the translations and dilations of Gabor functions with varying frequency orientations. Continuous Gabor wavelet transforms have been widely used in texture analysis and segmentation, whose discrete version is usually done via directly sampling the function on a discrete grid. The

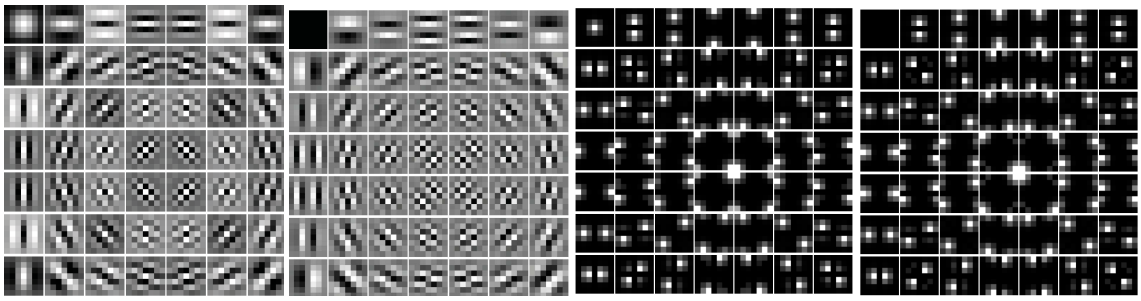

(a) Real(g_{ℓ_1,ℓ_2}) (b) Imag(g_{ℓ_1,ℓ_2}) (c) $|\widehat{\text{Real}(g_{\ell_1,\ell_2})}|$ (d) $|\widehat{\text{Imag}(g_{\ell_1,\ell_2})}|$

Fig. 2 Real and imaginary part of filter bank of a 2D tensor product Gabor frame constructed in Example 1 with size 7×7, and their discrete Fourier transforms. A filter is oriented in spatial domain if it is concentrated on a line in frequency domain.

system generated by such a simple discretization lacks some important property needed for sparsity-based image recovery methods, such as the fast numerical algorithm for exact reconstruction process. There is certainly the need to study the general theory of discrete version of Gabor systems from the very beginning.

In summary, the advantages of 2D Gabor functions on orientation selectivity, as well as powerful expressiveness on both cartoon image regions and texture image regions, motivated us to study the general theory of the discrete systems that are generated by the translations and modulations of a window function $g \in \mathbb{R}^N$. Such systems are indeed the so-called discrete *Gabor* (Weyl-Heisenberg) systems defined by

$$\{g[(m-ak) \bmod N]\mathrm{e}^{-2\pi i\ell bm} : m = 0, 1, ..., N-1\}_{k\in K,\ell\in L}, \tag{1}$$

where $a, \frac{1}{b} \in \mathbb{Z}$ denote the shift parameters and $K, L \subset \mathbb{Z}$ denote the integer lattices in finite time-frequency plane. 2D discrete Gabor systems are obtained via the tensor product of two 1D Gabor systems along each axis. Same as wavelet tight frames, the Gabor tight frames of the form (1) also have fast decomposition and reconstruction processes using 1D filter banks. However, the high-pass filters of its related filter banks have non-zero DC offsets which will cause un-desired artifacts in the results in applications. Thus, we also discussed the discrete Gabor frames whose associated high-pass filters have zero offsets while still having fast decomposition and reconstruction processes.

1.2 Outline of the work

The goal of this paper is to construct discrete Gabor frames that meet the needs from sparsity-based image recovery methods. Based on duality principle, a class of discrete Gabor frames with high orientation selectivity is constructed in this paper; see Fig. 2 for an illustration. In addition, the constructed discrete Gabor frames have fast implementation of both decomposition and reconstruction processes using 1D filter banks and the associate high-pass filters have zero DC offsets.

This paper is divided into two parts and they are organized as the following. The first part presents some results on Gabor frames for $\mathbb{C}^N$ which are used for constructing Gabor frames suitable for image recovery. More specifically, based on the *duality principle* derived from the Gramian and dual Gramian analysis for discrete Gabor frames for $\mathbb{C}^N$, we presented a sufficient and necessary condition for discrete Gabor tight frames, and used them to construct two classes of discrete tight Gabor frames. However, the proposed discrete tight frames cannot be directly used in sparsity-based image recovery methods, as the associated high-pass filters have non-zero DC offsets. Therefore, a new class of discrete Gabor frames with closed-form dual frames are derived which remove the non-zero DC offsets of all high-pass filters of tight Gabor frames.

The second part is about applying the constructed discrete Gabor frames to solve various image recovery problems. Using the constructed discrete Gabor frames, we presented an ℓ_1-norm relating regularization model applicable to many image restoration tasks, which reads the input image as the composite of multiple layers, and each layer represents one image component that satisfies the analysis-based sparse prior under a discrete Gabor frame. At last, the experiments are carried on several sample images to illustrate the advantages of the proposed tight Gabor frames over some existing frames.

2 Related work and our contributions

We first introduce some definitions and notations related to Gabor systems and frames. Let $\langle\cdot,\cdot\rangle$ and $\|\cdot\|$ denote the usual inner product and 2-norm of the Hilbert space H. $\{v_n\}_{n\in I} \subset H$ is called a *Bessel sequence* if there exists a

positive constant B such that

$$\sum_{n\in I} |\langle f, v_n\rangle|^2 \le B\|f\|^2, \quad \forall\, f \in H.$$

A Bessel sequence becomes a *frame* for H if there also exists a positive constant A such that

$$A\|f\|^2 \le \sum_{n\in I} |\langle f, v_n\rangle|^2 \le B\|f\|^2, \quad \forall\, f \in H.$$

A/B is called the lower/upper frame bound. A frame $\{v_n\}_{n\in I}$ is called *tight frame* when $A = B = 1$. A sequence $\{v_n\}_{n\in I}$ is called a *Riesz sequence* if there exist two positive constants C_1, C_2 such that

$$C_1 \sum_{n\in I} |c_n|^2 \le \| \sum_{n\in I} c_n v_n\|_2^2 \le C_2 \sum_{n\in I} |c_n|^2, \quad \forall\, \{c_n\}_{n\in I} \in \ell^2(I).$$

where $\ell^2(I)$ denotes the space of square summable sequences with index I. When $C_1 = C_2 = 1$, the Riesz sequence $\{v_n\}_{n\in I}$ becomes an *orthonormal sequence*. The Riesz sequence (orthonormal) $\{v_n\}_{n\in I}$ is a *Riesz (orthonormal) basis* for H if its linear span is dense in H.

For a Bessel sequence $\{v_n\}_{n\in I}$ for H, its *synthesis* operator, $T : \ell^2(I) \to H$ is defined by

$$Tc = \sum_{n\in I} c_n v_n \quad \forall\, c \in \ell^2(I) \tag{2}$$

and its adjoint operator, called *analysis* operator $T^* : H \to \ell^2(I)$ is defined by

$$T^* f(n) = \langle f, v_n\rangle, \quad n \in I. \tag{3}$$

The *frame* operator $S : H \to H$ is then defined by $S = TT^*$. Given a frame $\{u_n\}_{n\in I}$ for H, the sequence $\{v_n\}_{n\in I}$ is called its dual frame if

$$f = T_v T_u^* f = T_u T_v^* f, \quad \forall\, f \in H. \tag{4}$$

A frame $\{u_n\}_{n\in I}$ and its dual $\{v_n\}_{n\in I}$ are called *bi-frames* for H. Given a frame $\{v_n\}_{n\in I}$ for H, its dual frame is not unique and the so-called *canonical* dual frame is given by $\{(TT^*)^{-1}v_n\}_{n\in I}$. Two sequences $\{u_n\}_{n\in I}$ and $\{v_n\}_{n\in I}$ are called *bi-orthogonal* sequences if

$$\langle u_n, v_m\rangle = \delta_{m-n}, \quad \forall\, m, n \in I.$$

In 1946, D. Gabor [21] proposed the localized time-frequency analysis to decompose signals in $L^2(\mathbb{R})$ over the so-called Gabor or Weyl-Heisenberg system that is generated by the translation and modulation of a given window function g: $\{g_{m,n}(x) = g(x - na)e^{2\pi imbx}\}_{m,n\in\mathbb{Z}}$, where $a, b \in \mathbb{R}$ denote the shift parameters in time-frequency plane. The window functions originally proposed by Gabor are the Gaussians that have a minimal spread in time-frequency plane. Since then, most efforts have been devoted to the study of Gabor theory for function space $L^2(\mathbb{R}^d)$ (see e.g. [8, 12, 23, 38]) and for the infinite dimensional discrete space $\ell^2(\mathbb{Z})$ or $\ell^2(\mathbb{Z}^d)$ (see e.g. [11, 28, 32]). While the results on $\ell^2(\mathbb{Z})$ are also applicable to discrete Gabor systems for the space of finite signals by viewing finite signals as the sequences in $\ell^2(\mathbb{Z})$, there are also studies of Gabor systems for the space of finite signals $\mathbb{R}^N$ or $\mathbb{C}^N$, which is usually defined by (1):

$$X = (K, L)_g = \{g_{k,\ell}[m] = g[(m - ak) \bmod N]e^{-2\pi i\ell bm}, m = 0, 1, \ldots, N-1\}_{k\in K,\ell\in L}.$$

Here, $K, L \subset \mathbb{Z}$ are the pair of integer lattices of finite time-frequency plane. In the next, we give a brief review on the existing results of Gabor theory for $\mathbb{C}^N$ and outline our contributions.

2.1 Characterizations and constructions of discrete Gabor (tight) frames

For discrete Gabor systems for $\mathbb{C}^N$ defined by (1), there have been various characterizations presented in the past for discrete Gabor frames and tight Gabor frames. A necessary condition on the frame property of a discrete Gabor system for $\mathbb{C}^N$ or $\ell^2(\mathbb{Z})$ is $ab \le 1$ to ensure the cardinality of the system is no less than N. The so-called Wexler-Raz duality condition for $\mathbb{C}^N$ ([29, 46]) gives a necessary and sufficient condition on Gabor bi-frames on specific finite time-frequency lattices. Many fundamental facts of tight Gabor frames and Gabor frames for $\mathbb{C}^N$ are provided in Feichtinger et al. [20], which uses twisted group algebras as main tools. Feichtinger et al. [20] studied Gabor frames for finite signals over a finite Abelian group generated by an arbitrary lattice in finite time-frequency plane, and it covers many existing results on Gabor analysis for both product lattices and non-product lattices, including the *duality principle* [36, 38] which relates frame properties of a Gabor system to that of its adjoint system. In [19], the duality principle was generalized to the abstract Hilbert space for one single system, and further in [18],

the conclusion was extended to bi-systems. The studies for Gabor systems in $\ell^2(\mathbb{Z})$ and $\mathbb{C}^N$ can be seen as their specialization.

In this paper, we use the Gramian and dual Gramian analysis first developed in [38] for function spaces as the main tools to relate all frame properties of discrete Gabor systems to the analysis of the eigenvalues of their corresponding Gramian and dual Gramian matrices. Once the Gramian and dual Gramian analysis are established, the derivations of many existing results on discrete Gabor frames become straightforward, including the duality principle. The simplicity of such an approach comes from the fiberization technique introduced in [38]. While the frame properties of Gabor frames for function space requires almost all fibers have such frame properties, the frame properties of discrete Gabor frames only requires a given set of fibers have such frame properties. Therefore, one may sample a Gabor frame for $L^2(\mathbb{R})$ to get a discrete Gabor frame for $\ell^2(\mathbb{Z})$. In fact, this is what many existing schemes have done for constructing discrete Gabor frames for the space of finite signals; see e.g [24, 33, 41]. The main difference among these methods lies in the conditions used in the discrete sampling to generate a frame. For example, it is shown in [24] that the certain regularization condition should be imposed on the window function in order to form a frame for $\ell^2(\mathbb{Z})$ by sampling a Gabor frame for $L^2(\mathbb{R})$ with integer shift parameters. Moreover, it is shown in [24] that if the inner product of window function and its time-frequency shift has some decay, the minimal energy dual window can be sampled as well, preserving the duality and minimality.

Other existing approaches to construct the discrete Gabor bi-frames is either implicitly using the duality principle for bi-frames, i.e. the bi-orthogonality condition of the adjoint frame and its dual, or using the definition of canonical dual frame which is done either by solving a linear system or by using unitary matrix factorization of frame operator. Interesting readers are referred to [26,32,34,35,46] for more details. The discrete Gabor frames constructed by these methods usually do not have closed-form dual frames. Thus it needs to solve a linear system to find its dual which could be troublesome when the dimension of signals is very high. Using the fact that the Zak transform diagonalizes the analysis operator of a Gabor system when ab is 1 or reciprocal of an integer, an effective computation scheme is proposed in [1] for calculating a dual frame of a Gabor frame by using the Zak transform and the inverse Zak transform. A class of orthogonal and bi-orthogonal windowed Fourier bases, brush bases, are proposed in [31] for local time-frequency analysis. The focus of [31] is on the design of smooth positive window function, and the discrete version is done by sampling the systems in discrete grid. There have been few approaches for constructing discrete tight Gabor frame. In [11], a discrete Gabor tight frame is expressed from the viewpoint of a filter bank and thus the construction of tight Gabor frames is equivalent to the construction of paraunitary polyphase matrices, whose involved computation is non-trivial.

Using the duality principle, we first derive a necessary and sufficient condition for Gabor systems with non-negative window function to form tight frames for $\mathbb{C}^N$, followed by the constructions of two classes of tight Gabor frames generated by sampling two types of window functions satisfying the property of *partition of unity*: the square root of B-splines and the Fourier transform of scaling functions of Meyer wavelets. It is noted that partition of unity has also been used for constructing Gabor frames of function spaces; see e.g. [9]. However, the constructed Gabor tight frames are not suitable for image recovery, as the associated high-pass filter bank has non-zero DC offsets, i.e., the mean value of each atom is not zero. Therefore, a new class of Gabor frames is proposed by removing the DC offsets of all high-pass filters. Although the new discrete Gabor frames are not tight, their associated decomposition and reconstruction processes remain as simple as Gabor tight frames.

2.2 Sparse model based image recovery

In recent years, by assuming images of interest can be sparsely approximated under a frame or tight frame, sparsity-prompting functional (e.g. ℓ_1 norm) based regularization has been used in many image recovery tasks; see e.g. shift-invariant Daubechies wavelet system for image denoising [10], splines wavelet frame based image restoration methods [2, 5, 6] and curvelet based image recovery methods [42, 43]. Several approaches have been proposed for utilizing the sparse approximation of images, including synthesis approach, analysis approach and balanced approach. Interesting readers are referred to [16,40] for more details. There exist deep connections between wavelet frames based regularization method and the widely used total variation based regularization. Indeed, it is shown in [4] that the wavelet frame based analysis approach can be seen as sophisticated discretization of minimizations involving the total variation penalty.

Natural images are often composed of both cartoon and texture parts. Thus, a more efficient approach is viewing such images as the composite of multiple layers with different characteristics. Two-layer models are considered in [6,17] for image inpainting, in which one layer represents cartoon parts that are sparse in the domain of transforms such as wavelet, curvelet, ridgelets or contourlets, and the other layer represents texture parts that are sparse in the domain of transforms such as local DCT, Gabor or wavelet packets. The proposed discrete Gabor frames have their origins from local time-frequency analysis. Thus, they can deal with both cartoon parts and textural parts by using the window functions of varying supports.

To demonstrate the benefits of the discrete Gabor frames constructed in this paper for image recovery, we developed a multi-scale Gabor frame based regularization method for solving ill-posed linear inverse problem in image

recovery. Our regularization model follows the idea proposed in [6] for image inpainting, i.e., the image is read as the composite of multiple layers, and each layer represents image parts that can be sparsely modeled by the discrete Gabor frame with a particular scale. More specifically, consider the following signal recovery problem:

$$f = Hu + n, \tag{5}$$

where f is the degraded observation of true image u, H is the degradation matrix and n denotes noise. Let T_i^* denote the analysis operator of the discrete Gabor frame with respect to the ith scale. Then, we proposed the following regularization model for solving the linear inverse problem (5):

$$\{u_i\}_{i=1}^n := \text{argmin}_{\{v_i\}_{i=1}^n} \sum_{i=1}^n \lambda_i \|T_i^* v_i\|_1 \quad \text{s.t.} \quad \|H(\sum_{i=1}^n v_i) - f\|_2 \leq \epsilon, \tag{6}$$

where $\lambda_i, i = 1, \ldots, n$ denote some pre-defined regularization parameters. The recovered result u is then given by $u = \sum_{i=1}^n u_i$.

3 Constructions of discrete Gabor (tight) frames for image recovery

3.1 Gramian and dual Gramian analysis, fiberization and duality principle

Before the discussion, we first introduce some notations and definitions related to Gramian and dual Gramian analysis for Gabor systems. Let $g \in \mathbb{R}^N$ denote a window function with the length of support $p \leq N$, and let (a, b) denote two shift parameters in finite time-frequency plane with both a and b^{-1} being positive integers. Consider a Gabor system defined by

$$X = (K, L)_g = \{g_{k,\ell}[m] = g[(m - ak) \bmod N]\mathrm{e}^{-2\pi i \ell b m}, m = 0, 1, \ldots, N-1\}_{k \in K, \ell \in L}, \tag{7}$$

where $K, L \subset \mathbb{Z}$ are two lattices in finite time-frequency plane. The density of X is defined as $\mathrm{den}X = \frac{|K||L|}{N}$ where $|\cdot|$ denotes the cardinality of a set. X is clearly a Bessel sequence of $\mathbb{C}^N$, as well as a frame sequence of $\mathbb{C}^N$. The *pre-Gramian* of X defined in this paper, denoted by J_X, is an N-by-$|K||L|$ matrix given by

$$J_X[m, j(k, \ell)] = g_{k,\ell}[m], \quad 0 \leq m < N, \, 0 \leq j(k, \ell) < |K||L|, \tag{8}$$

which collects all elements of X column-wise. It is consistent with the definition of pre-Gramian defined in [18] and [19] using canonical orthonormal basis of $\mathbb{C}^N$. After defining the pre-Gramian, we define the *Gramian matrix* of X by $G_X = J_X^* J_X$ and the *dual Gramian matrix* by $\widetilde{G}_X = J_X J_X^*$. For two Gabor systems X, Y, we define their *mixed Gramian matrix* by $G_{X,Y} = J_X^* J_Y$, and their *mixed dual Gramian matrix* by $\widetilde{G}_{X,Y} = J_Y J_X^*$.

For a system X, its frame properties are closely related to the eigenvalues of its Gramian G_X and dual Gramian $\widetilde{G}_X$. Indeed, from the definition of pre-Gramian given in (8), it can be seen that J_X is exactly the synthesis operator T_X defined as (2) and the analysis operator T_X^* is the conjugate transpose of T_X. Thus, the frame properties of X can be described by the eigenvalues of G_X and $\widetilde{G}_X$. Let $\lambda(G)$ denotes the set of all eigenvalues of a matrix G. Then,

(i) X is a frame for $\mathbb{C}^N$ if and only if all eigenvalues of $\widetilde{G}_X$ are non-zero.
(ii) X is a tight frame for $\mathbb{C}^N$ if and only if all eigenvalues of $\widetilde{G}_X$ equal to 1.
(iii) X and Y are bi-frames for $\mathbb{C}^N$ if and only if $\widetilde{G}_{X,Y} = \widetilde{G}_{Y,X} = I$.
(iv) X is a Riesz sequence of $\mathbb{C}^N$ if and only if all eigenvalues of G_X are non-zero.
(v) X is an orthogonal sequence of $\mathbb{C}^N$ if and only if $G_X = I$.
(vi) X and Y are bi-orthogonal sequences of $\mathbb{C}^N$ if and only if $G_{X,Y} = G_{Y,X} = I$.

Clearly, the frame properties of a system X can be completely characterized from the eigenvalues of G_X and $\widetilde{G}_X$.

Recall that the columns of J_X are the elements of X. Consider another system X^* defined by all rows of J_X up to unitary equivalence, i.e. $J_{X^*} = V_1 J_X^* V_2$ where V_1 and V_2 are two unitary matrices. Such a system X^* is called an *adjoint system* of X in [18] and [19], as the dual Gramian matrix $\widetilde{G}_X$ of X is the Gramian matrix G_{X^*} of X^* up to unitary equivalence. In other words, all frame properties of a system X (e.g. frame property, frame bound and tight frame property) determined by its dual Gramian matrix $\widetilde{G}_X$ now can be also derived from the Gramian matrix G_{X^*} of X^*. Such a connection is the essential ingredient of the so-called *duality principle* ([18, 19, 36, 38]). In general, for a Gabor system, the adjoint system defined as above is not a Gabor system. In the next, we will consider another type of adjoint systems which are Gabor systems themselves.

For the simplicity of discussion, we consider that the length of signal N can be divided exactly by two shift parameters a and b^{-1}. Then an often seen lattice set $\{K, L\}$ of a Gabor system $X = (K, L)_g$ is given as follows,

$$K := \mathbb{N}^{N/a} = \{0, 1, \ldots, N/a - 1\}, \quad \text{and } L := \mathbb{N}^{\frac{1}{b}} = \{0, 1, \ldots, b^{-1} - 1\}. \tag{9}$$

Before discussing its adjoint Gabor system and the duality principle, we introduce a fiberization technique which can greatly simplify the analysis of the Gramian matrix and dual Gramian matrix of a Gabor system. The fiberization matrices of the pre-Gramian J_X, denoted by $J_X(m) \in \mathbb{C}^{bN\times\frac{N}{a}}$, is defined by

$$J_X(m)[\ell^*,k] = b^{-\frac{1}{2}} g[(m-b^{-1}\ell^*-ak) \bmod N], \quad 0\le \ell^* \le bN-1, 0\le k\le N/a-1, \tag{10}$$

for $m = 0,1,\dots,N-1$. Then, the fiberization matrices for the Gramians $G_X, \widetilde{G}_X, G_{X,Y}, \widetilde{G}_{X,Y}$ is defined by

$$\begin{cases} G_X(m) = J_X(m)^* J_X(m), \quad \widetilde{G}_X(m) = J_X(m)J_X(m)^*; \\ G_{X,Y}(m) = J_X(m)^* J_Y(m), \, \widetilde{G}_{X,Y}(m) = J_Y(m)J_X(m)^*, \end{cases} \quad \text{for } 0\le m<N. \tag{11}$$

Then, a direct extension of the fiberization technique introduced in [38] for continuous setting to the discrete setting leads to the following proposition.

Proposition 1 *Let $X = (K,L)_g$ denote a Gabor systems defined on the lattices (K,L) given by (9). Then there exist two unitary matrices $V_1 \in \mathbb{C}^{\frac{N}{ab}\times\frac{N}{ab}}$ and $V_2 \in \mathbb{C}^{N\times N}$ such that*

$$\begin{cases} V_1 G_X V_1^* = \operatorname{diag}(G_X(0), G_X(1), \dots, G_X(b^{-1}-1)); \\ V_2 \widetilde{G}_X V_2^* = \operatorname{diag}(\widetilde{G}_X(0), \widetilde{G}_X(1), \dots, \widetilde{G}_X(b^{-1}-1)). \end{cases} \tag{12}$$

where $G_X(m), \widetilde{G}_X(m), m = 0,\dots,b^{-1}-1$ are fiberization matrices given by (11).

Proposition 1 shows that up to unitary equivalence, the Gramian matrix G_X and dual Gramian matrix $\widetilde{G}_X$ can be re-written as block diagonal matrices of fiberization matrices. Thus, all frame properties of X now can be determined by analyzing the union of the eigenvalues of $\frac{1}{b}$ fiberization matrices of small size: $G_X(m) \in \mathbb{C}^{\frac{N}{a}\times\frac{N}{a}}, \widetilde{G}_X(m) \in \mathbb{C}^{Nb\times Nb}, m = 0,\dots,\frac{1}{b}-1$, which is easier to analyze than the big matrices G_X and $\widetilde{G}_X$.

Moreover, by a direct calculation, it can be seen that the transpose of fiberization matrices $J_X(m)$ defined by (10) is indeed the fiberization matrices of another Gabor system X^* (up to a constant), i.e.,

$$J_{X^*}(m) = (ab)^{\frac{1}{2}}\overline{J_X(m)^*}, \quad m = 1,2,\dots,N-1, \tag{13}$$

where $X^* = (L^*,K^*)_g$ is the Gabor system defined by the same window function g but with different shift parameters and different lattices:

$$L^* = \mathbb{N}^{Nb} = \{0,1,\dots,Nb-1\}, \quad \textit{and} \quad K^* = \mathbb{N}^a = \{0,1,\dots,a-1\}. \tag{14}$$

Thus, by the definition (11) of fiberization for Gramian and dual Gramian, there exists a connection between the dual Gramian $\widetilde{G}_X$ of $X = (K,L)_g$ and the Gramian G_{X^*} of $X^* = (L^*,K^*)_g$ given by (14). In other words, the Gabor system $X^* = (L^*,K^*)_g$ is an adjoint system of X, which is connected to X via duality principle as stated in the following proposition.

Proposition 2 *Let $X = (K,L)_g$ and $Y = (K,L)_{\widetilde{g}}$ be two Gabor systems for $\mathbb{C}^N$ defined on the lattices given by (9). Let $X^* = (L^*,K^*)_g$ and $Y^* = (L^*,K^*)_{\widetilde{g}}$ be the corresponding adjoint systems defined on the lattices given by (14). Then we have*

(i) X is a frame for $\mathbb{C}^N$ if and only $(ab)^{-\frac{1}{2}}X^*$ is a Riesz sequence of $\mathbb{C}^N$.

(ii) X is a tight frame for $\mathbb{C}^N$ if and only if $(ab)^{-\frac{1}{2}}X^*$ is an orthonormal sequence of $\mathbb{C}^N$.

(iii) X and Y are bi-frames for $\mathbb{C}^N$ if and only if $(ab)^{-\frac{1}{2}}X^*$ and $(ab)^{-\frac{1}{2}}Y^*$ are bi-orthogonal sequences of $\mathbb{C}^N$.

The connection between X and its adjoint Gabor system X^* stated in Proposition 2 shows that the construction of a Gabor tight frame X can be done via constructing a Gabor system X^* which is orthonormal sequence. Often, the construction and the analysis of orthonormal sequences are easier and simpler than that of tight frames. The advantages by working on the adjoint system X^* are exploited when deriving frame bounds of discrete Gabor frames, as well as a sufficient and necessary condition for Gabor tight frames with non-negative window functions.

Remark 1 Fiberization matrices for Gabor systems can also be defined in frequency domain. Similar to the case of functional space [38], we define

$$\hat{J}(\omega)[k^*,l] = a^{-\frac{1}{2}}\hat{g}(\omega/N + \frac{k^*}{a} + b\ell) \quad k^* \in K^*, l\in L,$$

for $\omega \in \mathbb{Z}^N$. Then, X and X^* have the same relationship as (13) via $\hat{J}(\omega)$:

$$\hat{J}_{X^*}(\omega) = (ab)^{\frac{1}{2}}\overline{\hat{J}_X(\omega)^*} \qquad \omega \in \mathbb{Z}_N.$$

Let F denote the discrete Fourier transform given by $F[\omega,m] = e^{-2\pi i\frac{m\omega}{N}}, \omega,m \in \mathbb{Z}_N$. Define a block-wise diagonal matrix $\hat{U} = \operatorname{diag}(\hat{U}_l)_{l\in L}$ with the l-th block given by

$$\hat{U}_l[\omega,k] = e^{-2\pi i ak(\frac{\omega}{N}+bl)}, \quad \omega,k \in K.$$

Then, $\frac{\sqrt{a}}{N}\hat{U}J_X^*F^*$ is the same as the block diagonal matrix $\widehat{J}^* = \operatorname{diag}(\hat{J}_X(\omega)^*)_{0\le\omega<N/a}$, up to permutations. As $\sqrt{\frac{a}{N}}\hat{U}$ and $\frac{1}{\sqrt{N}}F$ are both unitary matrices, the duality principle is established.

3.2 Construction of discrete Gabor tight frames

Many fundamental results of discrete Gabor frames can be easily obtained using the duality principle stated in Proposition 2. Corollary 1 and Corollary 2 listed below are essentially the results presented in [38] for function space in the discrete setting. For the self-containedness, we still provide the results and the proofs in this section.

Corollary 1 *Let X be a Gabor frame for $\mathbb{C}^N$. Then the frame bounds A, B of X satisfy*

$$\frac{A}{\|g\|_2^2} \leq \mathrm{den}X \leq \frac{B}{\|g\|_2^2}.$$

In particular, the windows function of a Gabor tight frame for $\mathbb{C}^N$ satisfies $\|g\|_2^2 = (\mathrm{den}X)^{-1} = ab$.

Proof Given a Gabor frame X for $\mathbb{C}^N$, its adjoint system X^* is then a Riesz sequence by Proposition 2. Let A^* and B^* denote its frame bounds. Then we have $T_{X^*}e_0 = g$ where e_0 denote the unit vector with first entry being 1. Thus, $A^* \leq \|T_{X^*}e_0\|_2^2 \leq B^*$ which gives $A^* \leq \|g\|_2^2 \leq B^*$.

X is a frame for $\mathbb{C}^N$ and its frame bounds A and B are characterised by the smallest and largest eigenvalues of G_X. From Proposition 1,

$$\begin{cases} A = \min_{m\in L}\{\min_\lambda \lambda(G_X(m))\} = \min_{m\in L}\{\min_\lambda \lambda(\widetilde{G}_X(m))\}, \\ B = \max_{m\in L}\{\max_\lambda \lambda(G_X(m))\} = \max_{m\in L}\{\max_\lambda \lambda(\widetilde{G}_X(m))\}; \end{cases}$$

Similar relation is true for A^*, B^* and eigenvalues of $G_{X^*}(m)$, $\widetilde{G}_{X^*}(m)$.

By checking the entries of G_X, we have for any $m \in L$,

$$G_X(m)[k', k] = G_X(m + b^{-1})[k', k], \quad 0 \leq k', k \leq \frac{N}{a} - 1,$$

and

$$\widetilde{G}_X(m)[l^{*\prime}, l^*] = \widetilde{G}_X(m + b^{-1})[(l^{*\prime} + 1) \bmod bN, (l^* + 1) \bmod bN], \quad 0 \leq l^{*\prime}, l^* \leq bN - 1.$$

Thus, for each $m \in L$, $G_X(m)$ and $G_X(m + b^{-1})$ are exactly the same, and $\widetilde{G}_X(m)$ and $\widetilde{G}_X(m + b^{-1})$ are also the same, up to the multiplication of some permutation matrix. Therefore,

$$\begin{cases} \cup_{m\in L}\lambda(G_X(m)) = \cup_{m\in\mathbb{Z}_N}\lambda(G_X(m)), \\ \cup_{m\in L}\lambda(\widetilde{G}_X(m)) = \cup_{m\in\mathbb{Z}_N}\lambda(\widetilde{G}_X(m)). \end{cases} \tag{15}$$

The similar conclusion holds true for X^*. Notice that $\widetilde{G}_{X^*}(m) = ab\overline{G_X(m)}$ for $m \in \mathbb{Z}_N$. Therefore, we obtain

$$\begin{cases} \cup_{m\in K^*}\lambda(\widetilde{G}_{X^*}(m)) = ab\cup_{m\in L}\lambda(G_X(m)), \\ \cup_{m\in K^*}\lambda(G_{X^*}(m)) = ab\cup_{m\in L}\lambda(\widetilde{G}_X(m)), \end{cases} \tag{16}$$

which implies $A^* = (\mathrm{den}X)^{-1}A$ and $B^* = (\mathrm{den}X)^{-1}B$. We have then

$$\frac{A}{\mathrm{den}X} = A^* \leq \|g\|_2^2 \leq B^* = \frac{B}{\mathrm{den}X}.$$

Thus, $A \leq \mathrm{den}X\|g\|_2^2 \leq B$.

Suppose that the window function g is non-negative with its support on a finite interval, which usually holds true in practice. Then, using the statement (iii) in Proposition 2, we have the following sufficient and necessary condition for X to form a tight frame for $\mathbb{C}^N$.

Corollary 2 *Suppose that $g \in \mathbb{R}^N$ is a non-negative vector with support $[0, p-1]$. Then, the Gabor system $X = (K, L)_g$ is a tight frame for $\mathbb{C}^N$ if and only if the following two conditions hold true:*

$$\text{(i)} \quad b \leq p^{-1}; \quad \textit{and} \quad \text{(ii)} \quad \sum_{k=0}^{N/a-1} (g[(\cdot - ak) \bmod N])^2 \equiv b.$$

Proof Suppose that X is a tight frame for $\mathbb{C}^N$. Then, X^* is an orthogonal sequence by the duality principle (Proposition 2). By contradiction, suppose that $b > p^{-1}$, then consider the following two elements in X^*: $\{g[m]\}$ and $\{g[(m - \frac{1}{b}) \bmod N]\}$. Then their inner product

$$\sum_{m=0}^{N-1} g[m]g[(m - \frac{1}{b}) \bmod N] \geq \sum_{m=1/b}^{p-1} g[m]g[m - \frac{1}{b}] > 0,$$

since g is non-negative and $g[m] > 0$ for $0 \le m \le p-1$, which contradicts the assumption that X^* is an orthogonal sequence. Thus, we have $b \le p^{-1}$. Moreover, by the definition of tight frame, we have $I = T_X T_X^*$. Notice that for $0 \le m, n \le N-1$,

$$\begin{aligned}(T_X T_X^*)[m,n] &= \sum_{k\in K, \ell \in L} g[(m-ak) \bmod N] g[(n-ak) \bmod N] e^{2\pi i \ell (n-m) b} \\ &= \begin{cases} 1/b \sum_{k\in K} (g[(m-ak) \bmod N])^2, & m = n; \\ 0, & m \ne n. \end{cases}\end{aligned}$$

Recall that $(T_X T_X^*)[m,m] = I[m,m] = 1$, which gives $\sum_{k\in K} (g[(\cdot - ak) \bmod N])^2 \equiv b$. Conversely, suppose that both conditions hold true. It can be seen that $(T_X T_X^*)[m,n] = 1$ if $m = n$ and 0 otherwise. Therefore, X is a tight frame for $\mathbb{C}^N$.

It can be seen from Corollary 2 that the construction of tight Gabor frames for $\mathbb{C}^N$ is simplified to finding a non-negative function g which satisfies the so-called *partition of unit* property, provided that b is set to be no larger than $1/p$. There are actually many such window functions with good regularity.

Example 1 Let B_n^a denote the B-spline of order n with the knots $\{0, a, \ldots, an\}$. Then, it is known ([15]) that the function B_n^a is a non-negative function with support $[0, an]$ and satisfies

$$\sum_{k\in\mathbb{Z}} B_n^a(t - ak) = 1, \qquad \forall\, t \in \mathbb{R},$$

which leads to $\sum_{k\in\mathbb{Z}} B_n^a(j-ak) = 1$ for any integer j. Define the vector g by $g(m) = \sqrt{b B_n^a(m)}$ for $m = 1, 2, \ldots, an-1$. Then it can be seen that $\sum_{k=0}^{N/a-1} |g[(\cdot - ak) \bmod N]|^2 = b$. Thus, the Gabor system $(K,L)_g$ generated by g with $b \le \frac{1}{an-1}$ is a tight frame for $\mathbb{C}^N$.

Example 2 Let ϕ denote the scaling function of Meyer wavelets defined by

$$\hat{\phi}(\omega) = \begin{cases} 1, & |\omega| \le \frac{2\pi}{3}; \\ \cos\left[\frac{\pi}{2}\beta\left(\frac{3}{2\pi}|\omega| - 1\right)\right], & \frac{2\pi}{3} \le |\omega| \le \frac{4\pi}{3}; \\ 0, & \text{otherwise,} \end{cases}$$

where β is a function satisfying $\beta(x) + \beta(1-x) = 1$ for $x \in [0,1]$. For example, the one used in [12] is given by $\beta(x) = x^4(35 - 84x + 70x^2 - 20x^3)$. It can be seen that

$$\sum_{k\in\mathbb{Z}} |\widehat{\phi}(\omega - 2k\pi)|^2 = 1, \quad \forall\, \omega \in \mathbb{R}.$$

Let $\widehat{\phi_a}(\omega) = \widehat{\phi}(\frac{2\pi\omega}{a})$. Then, $\sum_{k\in\mathbb{Z}} |\hat{\phi_a}(\cdot - ak)|^2 = 1$. Define the window function g by $g[m] = \sqrt{b}|\widehat{\phi_a}[m]|$. Then, a non-negative window function with partition of unity property is obtained, which leads to a tight frame $(K,L)_g$ for $\mathbb{C}^N$ if setting $b \le \frac{1}{p}$. For example, when $a = 4$, the vector g is given by $g = [1/\sqrt{2}, 1, 1, 1, 1/\sqrt{2}]$.

3.3 Construction of discrete Gabor frames for image recovery

The discrete tight frames constructed in the aforementioned section are not suitable for image recovery, as the associated filter banks have non-zero DC offsets. Thus, in this section, we derive a class of Gabor frames with zero DC offset and with closed-form dual frames.

3.3.1 Decomposition and reconstruction by filter banks

Discrete Gabor systems $X = (K,L)_g$ are closely connected to filter banks; see e.g. [1, 11]. For a signal $f \in \mathbb{C}^N$, let $\downarrow_a$ denote the down-sampling operator and $\uparrow_a$ denote the up-sampling operator defined by

$$\begin{aligned} &f_{\downarrow_a}[n] = f[an], \quad n = 0, 1, \ldots, \tfrac{N}{a} - 1; \\ &f_{\uparrow_a}[an] = f[n]; \quad n = 0, 1, \ldots \tfrac{N}{a} - 1, \quad \text{and all other elements of } f_{\uparrow_a} \text{ are zero.} \end{aligned}$$

For a filter $h \in \mathbb{C}^N$, there are two essential operators: one is the *analysis* operator $W_h : \mathbb{C}^N \to \mathbb{C}^{N/a}$ defined by

$$(W_h f)[j] = (\overline{h(-\cdot)} * f)_{\downarrow_a}[j] = \sum_{k=0}^{N-1} f[k] \overline{h[(k-aj) \bmod N]}.$$

and the other is the *synthesis* operator $W_h^* : \mathbb{C}^{N/a} \to \mathbb{C}^N$ defined by

$$(W_h^* c)[j] = (h * c_{\uparrow_a})[j] = \sum_{k=0}^{\frac{N}{a}-1} c[k]h[(j-ak) \bmod N].$$

The analysis operator T_X and the synthesis operator T_X^* of a Gabor system $X = (K, L)_g$ given by (7) can be expressed in terms of the set of analysis operators $\{W_{g_\ell}\}_{g_\ell \in \mathcal{G}}$ and the set of synthesis operators $\{W_{g_\ell}^*\}_{g_\ell \in \mathcal{G}}$, where $\mathcal{G}$ is a filter bank defined by

$$\mathcal{G} = \{g_\ell[m] = g[m]e^{-2\pi imb\ell}\}_{0 \le \ell \le 1/b-1}.$$

More specifically, let $D \in \mathbb{C}^{\frac{N}{ab}}$ denote the diagonal unitary matrix defined by

$$D = \operatorname{diag}(D_0, D_1, \ldots, D_{b^{-1}-1}), \tag{17}$$

where $D_\ell = \operatorname{diag}(1, e^{i\omega_0 \ell}, \ldots, e^{i\omega_0 \ell(\frac{N}{a}-1)})$ with $\omega_0 = 2\pi ab$. Then a direct calculation shows that the analysis operator T_X^* and the synthesis operator T_X can be re-written as

$$T_X^* = DW_X; \quad T_X = W_X^* D^*, \tag{18}$$

where $W_X : \mathbb{C}^N \to \mathbb{C}^{\frac{N}{ab}}$ denotes the analysis operator defined by the filter bank $\mathcal{G}$:

$$W_X f = \{c_0 = W_{g_0} f, c_1 = W_{g_1} f, \ldots, c_{\frac{1}{b}-1} = W_{g_{\frac{1}{b}-1}} f\}, \quad \forall\, f \in \mathbb{C}^N. \tag{19}$$

and $W_X^* : \mathbb{C}^{\frac{N}{ab}} \to \mathbb{C}^N$ denotes the synthesis operator defined by $\mathcal{G}$:

$$W_X^* c = \sum_{\ell=0}^{1/b-1} W_{g_\ell}^* c_\ell, \quad \forall c \in \mathbb{C}^{N/ab}. \tag{20}$$

It can be seen from (18) that the operator T_X (T_X^*) defined by X is the same as the operator W_X (W_X^*) defined from the filter bank $\mathcal{G}$, up to a diagonal matrix D with phase factors. It is noted that the phase factors only impact the phases of transform coefficients but keep their magnitudes unchanged. Thus, it will not impact the outcome when manipulating coefficients by a soft or hard thresholding operator. Therefore, adding or removing matrix D in the system does not have any impact in existing sparsity-based image recovery methods, as they only involve linear operations and thresholding operations on frame coefficients. Thus, in the remaining of this section, we focus on the analysis operator W_X and synthesis operator W_X^*.

The analysis operator W decomposes a signal f into multiple frequency sub-band channels, where $W_{g_0} f$ represents the low-frequence sub-band component and all other components $\{W_{g_\ell} f\}_{\ell=1}^{\frac{1}{b}-1}$ are high-frequency sub-band components. The filters $\{g_\ell\}_{\ell \neq 0}$ are windowed sinusoids that are only the approximation to high-pass filters, as none of their DC offsets (the summation of filter) are zero. As a result, the sub-band component decomposed by $g_{\ell \neq 0}$ contains a small percentage of low-frequency sub-band component, whose magnitude may be significant as image intensities are always non-negative. As natural images have sparse coefficients in high-frequency sub-bands but not in low-frequency sub-band, the effectiveness of sparse approximation under X could be noticeably degraded owing to non-zero DC offsets of these high-pass filters $\{g_\ell\}_{\ell \neq 0} \subset \mathcal{G}$.

Take the tight Gabor frames constructed in Example 1 for instance. Consider the tight Gabor frames constructed from cubic B-spline with nodes $[0, 1, 2, 3, 4]$ and $a = 1, b = 1/3$. Then, we have three filters with support 3:

$$g_0 = \frac{\sqrt{2}}{6}[1, 2, 1];\ g_1 = \frac{\sqrt{2}}{12}[2, -2, -1] + i\frac{\sqrt{6}}{12}[0, -2, 1];\ g_2 = \frac{\sqrt{2}}{12}[2, -2, -1] + i\frac{\sqrt{6}}{12}[0, 2, -1]. \tag{21}$$

It can be seen that the two high-pass filters g_1 and g_2 have non-zero DC offsets. The same holds true for other tight frames in Example 1 and Example 2. It is observed in the experiments that when using these high-pass filters with non-zero DC offset in sparsity-based image recovery, the results often show strong artifacts, especially in those smooth regions.

3.3.2 Gabor frames with filters of zero DC off-sets

Motivated by the needs from sparsity-based image recovery, we proposed a modified version of tight Gabor frames to remove the DC offsets of the corresponding high-pass filters. Although the resulting Gabor frames are not tight anymore, there exist closed-form dual frames with simple structures. The modification is done by keeping the low-pass filter g_0 and modifying high-pass filters $\{g_\ell\}_{\ell\neq 0}$ as the following: $\mathring{g}_\ell = e^{i\theta_\ell} g_\ell - \mu_\ell g_0$, for $\ell = 1, 2, \ldots, b^{-1}-1$, where $e^{i\theta_\ell}$ and μ_ℓ are chosen such that $\sum_m \mathring{g}_\ell(m) = 0$. In our implementation, $\{e^{i\theta_\ell}\}_{\ell\neq 0}$ and $\{\mu_\ell\}_{\ell\neq 0}$ are given by

$$e^{i\theta_\ell} = \overline{\sum_m g_\ell(m)}/|\overline{\sum_m g_\ell(m)}|; \quad \text{and } \mu_\ell = |\overline{\sum_m g_\ell(m)}|/\sum_m g_0(m). \tag{22}$$

Denote $\theta_0 = \mu_0 = 0$. It can be seen that the system Y corresponding to these modified high-pass filters are

$$Y = \{\mathring{g}_{k,\ell}\}_{k\in K,\ell\in L} = \{e^{i\theta_\ell} g_{k,\ell} - \mu_\ell e^{-2\pi i akb\ell} g_{k,0}\}_{k\in K,\ell\in L}. \tag{23}$$

Although the new Gabor system Y derived from X is no longer a tight frame, it has a closed-form dual frame with well-posed frame bounds. By the definition of $\{\mathring{g}_\ell\}_{\ell\in L}$,

$$W_Y = MW_X. \tag{24}$$

and the analysis operator T_Y^* of Y is then

$$T_Y^* = DMW_X, \tag{25}$$

where $M \in \mathbb{R}^{N\times \frac{N}{ab}}$ is given by

$$M = \begin{pmatrix} I_{\frac{N}{a}} & \mathbf{0} & \ldots & \mathbf{0} \\ -\mu_1 I_{\frac{N}{a}} & e^{-i\theta_1} I_{\frac{N}{a}} & & \\ \vdots & & \ddots & \\ -\mu_{\frac{1}{b}-1} I_{\frac{N}{a}} & & & e^{-i\theta_{\frac{1}{b}-1}} I_{\frac{N}{a}} \end{pmatrix},$$

and here $I_{\frac{N}{a}}$ denotes the $\frac{N}{a}\times\frac{N}{a}$ identity matrix. The matrix M is a sparse matrix with a sparse inverse:

$$M^{-1} = \begin{pmatrix} I_{\frac{N}{a}} & \mathbf{0} & \ldots & \mathbf{0} \\ e^{i\theta_1}\mu_1 I_{\frac{N}{a}} & e^{i\theta_1} I_{\frac{N}{a}} & & \\ \vdots & & \ddots & \\ e^{i\theta_{\frac{1}{b}-1}}\mu_{\frac{1}{b}-1} I_{\frac{N}{a}} & & & e^{i\theta_{\frac{1}{b}-1}} I_{\frac{N}{a}} \end{pmatrix}.$$

Define the system $\widetilde{Y} = \{\widetilde{g}_{k,\ell}\}_{k\in K,\ell\in L}$ by

$$\begin{array}{l} \widetilde{g}_{k,0} = g_{k,0} + \sum_{\ell\neq 0,\ell\in L} \mu_l e^{2\pi i akb\ell + i\theta_\ell} g_{k,\ell}, \quad k\in K; \\ \widetilde{g}_{k,\ell} = e^{i\theta_\ell} g_{k,\ell}, \quad k\in K, \ell\in L\backslash\{0\}. \end{array} \tag{26}$$

Then, the systhesis operator defined by $\widetilde{Y}$ which leads to $T_{\widetilde{Y}} = W_X^* M^{-1} D^*$ and gives

$$T_{\widetilde{Y}} T_Y^* = W_X^* M^{-1} D^* DMW_X = I.$$

Thus, Y and $\widetilde{Y}$ form dual frames for $\mathbb{C}^N$. It can be seen that the computational cost of the analysis operator T_Y^* and the synthesis operator $T_{\widetilde{Y}}$ is nearly the same as T_X^* and T_X.

Proposition 3 *Suppose that X is a discrete Gabor tight frame for $\mathbb{C}^N$ defined as (7). Then, Y and $\widetilde{Y}$ derived from X by (23) and (26) are dual frames for $\mathbb{C}^N$.*

Example 3 Consider the tight Gabor frame constructed from B-spline of order 3 whose three filters are listed in (21). The corresponding filters of the Gabor frame Y and its dual $\widetilde{Y}$ are now

$$\begin{cases} g_0 = \frac{\sqrt{2}}{6}[1,2,1]; \\ g_1 = \frac{\sqrt{2}}{8}[-1,2,-1] + i\frac{\sqrt{6}}{12}[1,0,-1]; \\ g_2 = \frac{\sqrt{2}}{8}[-1,2,-1] + i\frac{\sqrt{6}}{12}[-1,0,1], \end{cases} \quad \textit{and} \quad \begin{cases} \widetilde{g}_0 = \frac{\sqrt{2}}{8}[1,4,1]; \\ \widetilde{g}_1 = \frac{\sqrt{2}}{12}[-1,4,-1] + i\frac{\sqrt{6}}{12}[1,0,-1]; \\ \widetilde{g}_2 = \frac{\sqrt{2}}{8}[-1,4,-1] + i\frac{\sqrt{6}}{12}[-1,0,1]. \end{cases} \tag{27}$$

It can be seen that the filters g_1 and g_2 are both high-pass filters with zero DC offset. The frame bounds are $A = 0.8000$ and $B = 1.0000$. The redundancy is $3N/N = 3$.

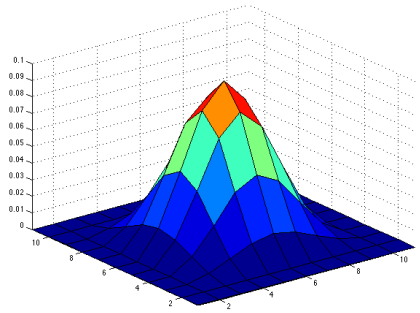

(a) Gabor atom of frame

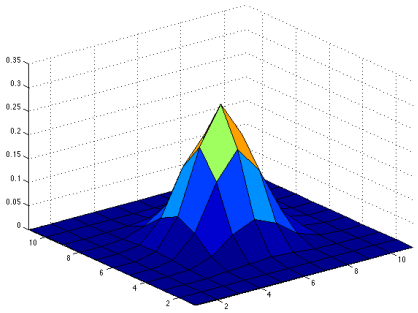

(b) Gabor atom of dual frame

Fig. 3 Gabor atoms of discrete Gabor frame constructed in Example 4 with respect to low-pass filters

Example 4 2D discrete Gabor frames can be generated by the tensor product of two 1D discrete Gabor frames along two axes. Consider the 1D Gabor tight frame constructed in Example 1 by using the B-spline of order 4 and setting $a = 2, b = 1/7$. Let Y denote the corresponding 1D Gabor frame after removing non-zero DC offsets in all high-pass filters. Then, the frame bounds of the resulting 2D discrete Gabor frames $Y \otimes Y$ are $A = 0.5443$ and $B = 1.0069$. The redundancy is $(\frac{7N}{2})^2/N^2 = 12.25$. The support of all associated filters is 7×7. The concentrations of the Gabor atoms associated with low-pass filters are illustrated in Fig. 3 for both frame and dual frame. The associated high-pass filters have good orientation selectivity as shown in Fig. 2.

3.4 Analysis of orientation selectivity

The orientation selectivity of 2D discrete filters are usually characterized by the peaks of their discrete Fourier transforms; see e.g. [31, 39]. Consider a continuous function $f(x, y) \in L^2(\mathbb{R}^2)$ of particular orientation θ that is expressed as

$$f(x, y) = h(x\cos\theta - y\sin\theta)\kappa(x, y),$$

where $h \in L^2(\mathbb{R})$ and $\kappa \in L^2(\mathbb{R}^2)$ is the isotrophic separable regularizer for $f \in L^2(\mathbb{R}^2)$ satisfying $\kappa(x, y) = g(x)g(y)$, e.g. Gaussian function $g(t) = \sqrt{2\pi\sigma}e^{-\frac{t^2}{2\sigma^2}}$. Then, we have

$$\begin{aligned}
\widehat{f}(\omega_x, \omega_y) &= \int_{\mathbb{R}}\int_{\mathbb{R}} h(x\cos\theta - y\sin\theta)\kappa(x, y)e^{-i(\omega_x x+\omega_y y)}dxdy \\
&= \int_{\mathbb{R}}\int_{\mathbb{R}} h(x)\kappa(x\cos\theta + y\sin\theta, -x\sin\theta + y\cos\theta)e^{-i(\omega_x(x\cos\theta+y\sin\theta)+\omega_y(-x\sin\theta+y\cos\theta))}dxdy \\
&= \int_{\mathbb{R}}\int_{\mathbb{R}} h(x)\kappa(x, y)e^{-i(\omega_x(x\cos\theta+y\sin\theta)+\omega_y(-x\sin\theta+y\cos\theta))}dxdy \qquad \text{(isotrophy)} \\
&= \int_{\mathbb{R}}\int_{\mathbb{R}} h(x)g(x)g(y)e^{-i(\omega_x(x\cos\theta+y\sin\theta)+\omega_y(-x\sin\theta+y\cos\theta))}dxdy \qquad \text{(separability)} \\
&= (\widehat{h} * \widehat{g})(\omega_x\cos\theta - \omega_y\sin\theta)\widehat{g}(\omega_x\sin\theta + \omega_y\cos\theta).
\end{aligned}$$

Suppose that $\widehat{g}$ decays fast when going away from origin, e.g., Gaussian functions. It can be seen that magnitude of $\widehat{f}(\omega_x, \omega_y)$ also decays fast when (ω_x, ω_y) is away from the line $\omega_x\sin\theta + \omega_y\cos\theta = 0$. Thus, the orientation of a function f is closely related to the peaks of its Fourier transform. To be specific, the peaks of the Fourier transform of an oriented function forms a line in frequency domain and its orientation is complementary to that of the function.

Motivated by the property of an oriented continuous function in frequency domain discussed above, the orientation selectivity of a discrete high-pass filter can also be defined in terms of the peaks of its discrete Fourier transform. For simplicity, consider an odd-length high-pass filter $g \in \mathbb{C}^{p\times p}$. Let $\mathbb{Z}_p \times \mathbb{Z}_p$ denote the discrete grid of its DFT with $\mathbb{Z}_p = \{-\frac{p-1}{2}, -\frac{p-1}{2}+1, ..., 0, ..., \frac{p-1}{2}\}$. Then a high-pass filter g is considered having perfect/strong selectivity with respect to the orientation θ if its DFT satisfies the following two conditions:

(1) all maximum points of $|\widehat{g}|$ are on the line $\omega_x\cos\theta + \omega_y\sin\theta = 0$ in frequency domain;
(2) the values of the points away from the line $\omega_x\cos\theta + \omega_y\sin\theta = 0$ are zero (perfect) or negligible (strong).

Clearly, the high-pass filters derived from both real part and imaginary part of 2D DFT have perfect orientation selectivity as the non-maximum points of their DFTs vanish outside the line. See Fig. 4 for an illustration. Similar to that from DFT, the high-pass filters derived from the proposed Gabor frames also have very strong orientation selectivity as the values of non-maximum points of their DFTs are much smaller than the maximum; see Fig. 2 for a comparison.

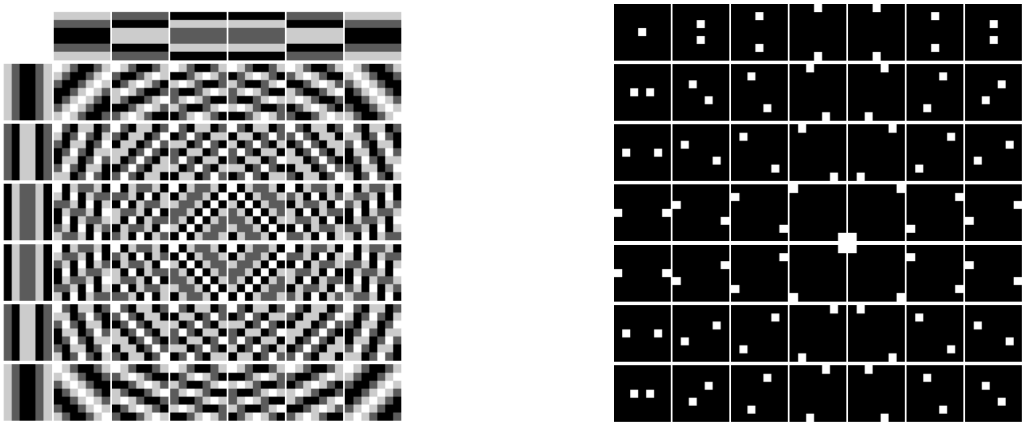

(a) Real(f_{j_1,j_2}) (b) $|\widehat{\text{Real}(f_{j_1,j_2})}|$

Fig. 4 Real part of 2D discrete Fourier basis $\{f_{j_1,j_2}\}_{0\le j_1,j_2\le 6}$ of size 7×7 and their Fourier spectrum.

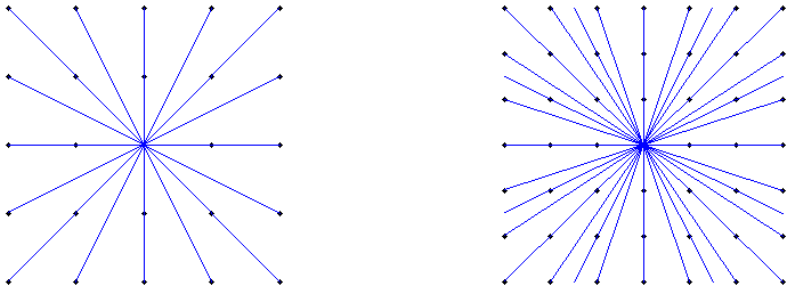

(a) 5×5 (b) 7×7

Fig. 5 All feasible orientations of 2D filters of size 5×5 and size 7×7.

In addition, the orientation selectivity of the high-pass filters from 2D DFT or from the proposed Gabor frames is optimal in the sense that they cover all possible orientations in finite discrete grid. One orientation is feasible for a finite discrete grid only if the line with such orientation can intersect the grid $\mathbb{Z}_p\times\mathbb{Z}_p$, which makes the number of all feasible orientations limited. It can be seen that for 2D filters of size 5×5, the total number of possible orientations is 8, and for 2D filters of size 7×7, the total number is 16; see Fig. 5 for an illustration. Indeed, by induction, the total number of feasible orientations for 2D filters of odd size $p\times p$ is $4\Phi(\frac{p-1}{2})$, where the function $\Phi(\cdot)$ is the summation function of the Euler's totient function $\varphi(\cdot)$ which counts the positive integer up to k that are relatively prime to k, i.e. $\Phi(n)=\sum_{k=1}^{n}\varphi(k)$. The derivation is quite straightforward. It can be seen that the number of all feasible orientations doubles that of the first quadrant of the grid with length $\frac{p-1}{2}$. The possible candidates of additional feasible orientations in the first quadrant from $k=p-1$ to $k=p$ are those come from the boundary points the grid. For such a point, if its x-coordinate or y-coordinate is relatively prime to $\frac{p-1}{2}$, then it induces a new orientation. Thus, the number of new feasible orientations induced from $k=p-1$ to $k=p$ in the first quadrant is $2\phi(\frac{p-1}{2}))$, and the total number is then $4\phi(\frac{p-1}{2})$. By induction, the proof is done.

4 Image recovery using discrete Gabor frames

A 2D image is a 2D array that can be understood as a vector in $\mathbb{R}^N$ where N is the total number of image pixels. Then the decomposition operator W of a 2D Gabor frame and the reconstruction operator $\widetilde{W}$ of its dual can be viewed as matrices in $\mathbb{C}^{\frac{N}{ab}\times N}$ and in $\mathbb{C}^{N\times\frac{N}{ab}}$ respectively. Image recovery is about solving a linear inverse problem:

$$f=Hu+n, \tag{28}$$

where f denotes the observed degraded image, u denotes the original image for recovery and n denotes noise. The operator H is the measuring matrix that varies in different image recovery problems. For image deblurring, H is a convolution operator with a low-pass filter. For image denoising, H is an identity matrix. For image in-painting, H is a diagonal matrix whose diagonal element is 1 when the corresponding pixel value is available and 0 otherwise.

4.1 Regularization models and numerical algorithms

For an input image composed of both cartoon parts and textural parts, we propose a sparsity-based multi-layer composite model which is based on multiple discrete Gabor frames generated by the window functions of different sizes. More specifically, we assume that the input image is composed of multiple layers in which each layer can be sparsely approximated under a discrete Gabor frame with a different window size. Based on such a sparsity-based multi-layer composite model of images, we propose the following regularization model for solving (28):

$$\min_{\{u_1,\ldots,u_m\}\subset\mathbb{R}^N} \sum_{k=1}^{m} \lambda_k \|W_{Y_k} u_k\|_1, \quad \text{s.t.} \quad \|H(\sum_{k=1}^{m} u_k) - f\|_2 \le \epsilon, \tag{29}$$

where W_{Y_k} denotes the decomposition operator of the Gabor system Y_k, ϵ denotes the tolerance determined by noise level and λ_k denotes the pre-defined regularization parameter. The recovered image $\hat{u}$ is then synthesized by u_ks via $\hat{u} = \sum_{k=1}^{m} u_k$. A more compact form of (29) is given by

$$\min_{u\in\mathbb{R}^{mN}} \|Wu\|_1, \quad \text{s.t.} \quad \|\widetilde{H}u - f\|_2 \le \epsilon, \tag{30}$$

where $u = [u_1^\top, \ldots, u_m^\top]^\top \in \mathbb{R}^{mN}$, $\widetilde{H} = [H, H, \ldots, H] \in \mathbb{R}^{N\times mN}$ and $W = \mathrm{diag}(\lambda_1 W_{Y_1}, \ldots, \lambda_m W_{Y_m}) \in \mathbb{R}^{\frac{mN}{ab}\times mN}$. The minimization problem (30) is an ℓ_1 norm related convex problem which has been extensively studied in recent years. It can be efficiently solved by the split Bregman iteration or equivalently the ADMM method via the following iteration:

$$\begin{cases} (\widetilde{H}^\top\widetilde{H} + \mu W^*W)u^{k+1} = \widetilde{H}^\top(f - c^k) + \mu W^*(d^k - b^k) \\ d^{k+1} = \mathcal{T}_{\frac{1}{\mu}}(Wu^{k+1} + b^k), \\ b^{k+1} = b^k + Wu^{k+1} - d^{k+1}, \\ c^{k+1} = c^k + \widetilde{H}u^{k+1} - f, \end{cases} \tag{31}$$

where $\mathcal{T}_\delta(w) = [t_\delta(w_1), t_\delta(w_2), \ldots]^\top$ is the soft thresholding operator, with $t_\delta(w_i) = \frac{w_i}{|w_i|}\max\{0, |w_i| - \delta\}$ if $w_i \neq 0$ and $t_\delta(0) = 0$. Interesting readers are referred to [6] for more details. In our implementation, the conjugate gradient method is called for solving the linear system in the first step of the iteration. It is noted that although W is a complex-valued operator, all intermediate variables u^{k+1}, c^{k+1} are real-valued. The reason is that the filters corresponding to the proposed Gabor frames always appear as conjugate pairs. In other words, the Gabor frame coefficients also appear as conjugate pairs. In addition, for any conjugate pair of coefficients, the thresholding operator t_δ either set both to 0 or keep them remaining as a conjugate pair. Thus, all intermediate variables are real-valued.

4.2 Image recovery and experimental evaluation

In this section, we apply multi-scale discrete Gabor frames based regularization model (29) to solve three typical image recovery problems: image denoising, image inpainting and image de-convolution. The implementation of the regularization method (29) is done as follows. The multi-scale discrete Gabor frames are composed of two Gabor systems constructed in Section 3.3.2 with two different scales. One Gabor frame is the discrete Gabor frame of the form (23) modified from the tight frame in Example 1 using the B-spline of order 4 with the nodes $[0, 2, 4, 6, 8]$. Two shift parameters of the lattices are $a = 2$ and $b = 1$. Another Gabor system is the large-scale version of the first one by sampling the same B-spline function of order 4 but with the nodes $[0, 4, 8, \ldots, 16]$. Two shift parameters of the lattices are $a = 4$ and $b = 1$. The filter size of the filter banks associated with these two systems are $p = 7$ and $p = 15$ respectively.

To illustrate the benefit of discrete Gabor frames constructed in Section 3.3.2 for sparsity-based image recovery, the results are compared to that from several other ℓ_1 norm based regularization methods which are based on different systems for sparsifying images. The first one is the popular TV based image restoration method (see e.g. [45]) that regularizes the image recovery by minimizing the total variation of the result. The next one is wavelet frame based method [6] which uses the same analysis model (30) and use linear spline tight wavelet frame [13, 37] as the sparsifying system. Also, a two-system based method is proposed in [6] for image denoising, which also uses the analysis model (30) but considers two systems: local DCT and linear spline wavelet frame. The third one is using the same regularization model (30) but the sparsifying system is the dual-tree complex wavelet (DT-CWT) [39] whose associated filter bank has up to six orientations. In the implementation of DC-CWT, near Symmetric $(13, 19)$ tap filters are chosen in the lowest level and Q-Shift $(10, 10)$ tap filters are chosen in two higher levels to gain the optimal performance. The last one also used the regularization model (30) but considered a different system, the extended

(a) Barbara (b) Bowl (c) Cameraman (d) Fingerprint (e) Lena

Fig. 6 Visualization of five tested images

Table 1 PSNR values of inpainted images

image	TV	framelet +LDCT	DTCWT	DST18	Gabor size:15,7
Barbara512	31.14	33.77	32.16	33.07	**35.55**
Bowl256	33.06	35.71	34.36	35.43	**36.24**
Cameraman256	28.81	29.83	29.70	29.50	**30.79**
Fingerprint512	25.26	28.30	**29.76**	**29.76**	29.29
Lena512	34.41	35.28	36.32	36.08	**36.90**

Table 2 PSNR values of denoised images

image	σ	TV	framelet +LDCT	DT CWT	DST18	Gabor size:15,7
Barbara512	20	26.84	29.25	28.90	29.55	**30.39**
	30	24.82	27.14	26.61	27.37	**28.23**
	40	23.87	25.78	24.91	25.94	**26.71**
	50	23.22	24.40	23.78	24.69	**25.40**
Bowl256	20	29.24	30.15	29.43	30.35	**30.58**
	30	27.63	28.51	27.50	28.54	**28.84**
	40	26.76	27.42	26.42	27.42	**27.81**
	50	26.15	26.68	25.64	26.48	**26.80**
Cameraman256	20	28.83	29.00	28.94	28.91	**29.26**
	30	26.83	27.18	26.92	26.96	**27.43**
	40	25.53	25.73	25.29	25.66	**26.00**
	50	24.50	24.55	24.06	24.61	**25.03**
Fingerprint512	20	26.60	27.79	28.01	28.05	**28.31**
	30	24.31	25.75	26.04	26.08	**26.16**
	40	22.91	24.08	24.65	**24.83**	24.63
	50	21.71	22.81	23.37	**23.76**	23.47
Lena512	20	30.71	31.10	31.49	**31.91**	31.74
	30	29.30	29.43	29.62	**30.02**	29.97
	40	28.09	27.78	28.20	28.45	**28.55**
	50	27.24	27.14	27.31	**27.75**	27.61

discrete shearlet transform[1] which uses 18 directions (DST18) [27]. The parameters involved in these methods are rigorously tuned up to achieve the best average performance over tested images. The performance of image recovery is measured in terms of the PSNR value given by

$$\text{PSNR} = -20\log_{10}\frac{\|u-\widetilde{u}\|}{255N},$$

where N denotes the number of pixels, u and $\widetilde{u}$ denote the truth and the result.

In the experiments of image inpainting, the observed images are synthesized by man-made masks without noise on five tested images shown in Fig. 6. The parameters of inpainting is uniformly set for all images: $\lambda_1 = 0.001$; $\lambda_2 = 0.002$ and $\mu = 0.005$. See Table 1 for the summary of the PSNR values of the results inpainted by different methods and Fig. 7 for the visual illustration of one sample image.

In the experiments of image denoising, the noisy images are synthesized by adding i.i.d. Gaussian white noise with different standard deviations: $\sigma = 20, 30, 40, 50$ on five tested images shown in Fig. 6. The parameters of denoising is uniformly set for all images by the empirical formulation: $\lambda_1 = \frac{\sigma^2}{80} - \frac{\sigma}{5} + 13$; $\lambda_2 = -\frac{\sigma^2}{400} + \frac{7\sigma}{5} - 10$ and $\mu = \frac{1}{2}\sigma$. See Table 2 for the summary of the PSNR values of the results denoised by different methods. It can be seen that the performance of the proposed Gabor frame based method is overall better than the other four methods on tested images. The improvement in terms of PSNR value is also consistent with the improvement in terms of visual quality; see Fig. 8 for a visual illustration of the results obtained by different methods.

In the experiments of image deconvolution, the tested images are synthesized by first blurring the images by a blur kernel and then adding i.i.d. Gaussian white noise afterward. Together with two noise levels $\sigma = 3, 5$, four types of blur kernel are tested: 1) disk kernel of radius 3 pixels, 2) linear motion blur kernel of length 15 pixels and of orientation 30°, 3) Gaussian kernel of size 15×15 pixels and standard derivation 2, and 4) averaging kernel

[1] http://www3.math.tu-berlin.de/numerik/www.shearlab.org/software

(a) image with missing data (b) TV (c) framelet and Local DCT

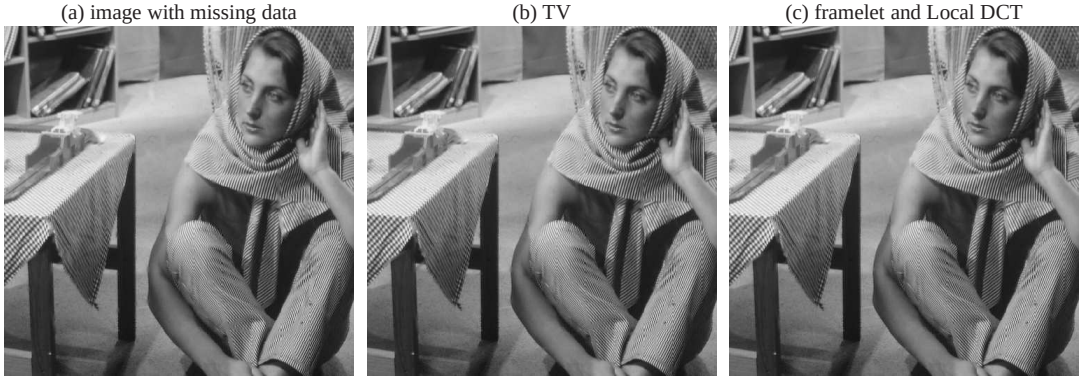

(d) DT-CWT (e) shearlet (f) discrete Gabor frame

Fig. 7 Visual illustration of image inpainting. (a) observed image with missing pixels and noise level $\sigma = 0$; (b)-(f) inpainted results by five different methods.

(a) noisy image (b) TV (c) framelet and Local DCT

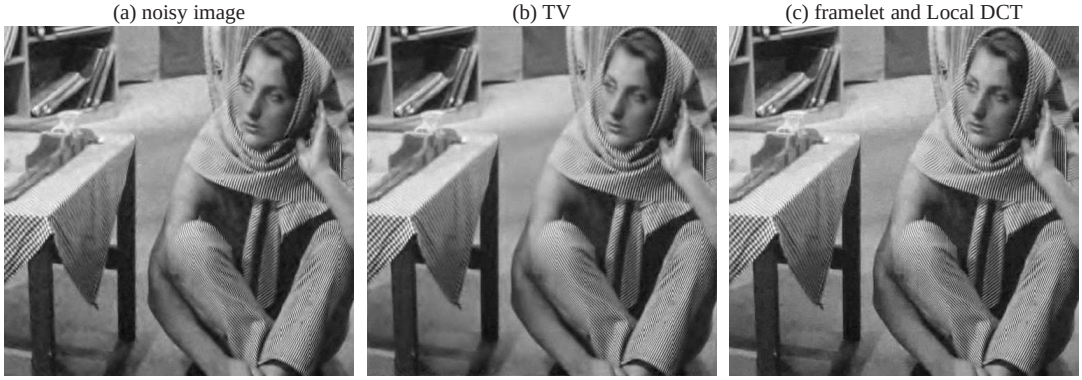

(d) DT-CWT (e) shearlet (f) discrete Gabor frame

Fig. 8 Visual illustration of image denoising. (a) noisy image with noise level $\sigma = 20$; (b)-(f) denoised results by five different methods.

Table 3 PSNR values of deblurred results for blurred images with noise level $\sigma = 3$ and 5

image	blur kernel	$\sigma = 3$					$\sigma = 5$				
		TV	framelet	DT-CWT	DST18	Gabor size:15,7	TV	framelet	DT-CWT	DST18	Gabor size:15,7
Barbara512	disk	24.77	25.17	25.15	25.27	**25.65**	24.28	24.41	24.37	24.52	**24.78**
	motion	24.64	24.97	25.00	25.11	**25.70**	24.06	24.13	24.18	24.20	**24.48**
	Gaussian	24.13	24.14	24.19	24.12	**24.21**	23.96	23.99	24.01	23.94	**24.02**
	average	23.99	24.03	24.07	24.07	**24.27**	23.67	23.67	23.72	23.73	**23.87**
Bowl256	disk	28.73	28.92	28.99	28.94	**29.35**	28.01	28.08	28.25	28.14	**28.48**
	motion	28.88	29.08	29.15	29.31	**29.67**	27.68	27.92	27.93	27.93	**28.36**
	Gaussian	27.96	27.82	28.32	28.27	**28.66**	27.47	27.35	27.61	27.65	**27.81**
	average	28.73	28.84	28.94	28.99	**29.25**	27.84	27.75	28.10	28.25	**28.44**
Cameraman256	disk	26.31	26.83	26.22	25.98	**27.01**	25.40	**25.62**	24.99	24.97	25.60
	motion	26.18	**27.14**	26.35	25.98	26.93	24.89	25.36	24.77	24.59	**25.41**
	Gaussian	24.96	24.84	24.73	24.62	**25.04**	24.55	24.43	24.34	24.23	**24.61**
	average	25.08	25.12	25.00	24.74	**25.55**	24.25	24.07	24.11	23.88	**24.57**
Fingerprint512	disk	27.71	27.38	28.19	28.02	**28.24**	26.69	26.43	**27.25**	27.01	27.21
	motion	25.40	24.66	**26.35**	26.16	26.03	23.95	23.36	**24.88**	24.65	24.44
	Gaussian	27.15	27.07	27.37	27.20	**27.49**	26.23	26.20	26.51	26.39	**26.56**
	average	24.16	23.84	**24.85**	24.76	24.76	23.07	22.81	**23.79**	23.76	23.63
Lena512	disk	32.05	32.17	32.25	31.87	**32.53**	31.13	31.26	31.27	30.68	**31.42**
	motion	30.86	30.49	31.21	30.93	**31.43**	29.54	29.53	29.86	29.25	**29.93**
	Gaussian	31.34	31.26	31.59	31.18	**31.74**	30.60	30.58	30.77	30.38	**30.83**
	average	30.10	29.96	30.21	29.95	**30.36**	29.27	29.13	29.37	29.03	**29.48**

(a) blurred image (b) TV (c) framelet

(d) DT-CWT (e) Shearlet (f) discrete Gabor frame

Fig. 9 Visual illustration of image deconvolution. (a) image blurred by motion kernel and added by noise with noise level $\sigma = 3$; (b)-(f) deblurred results by different methods.

of size 9×9 pixels. Through the experiments, the parameter of (31) is uniformly set for all images as follows: $\lambda_1 = \lambda_2 = \frac{\sigma^2}{5} + 3\sigma - 1$ and $\mu = \frac{\sigma}{10}$. See Table 3 for the summary of PSNR values of results deblurred by different methods. It can be seen that the proposed method generally outperformed other methods used for comparison. The same improvement also holds in terms of visual quality; see Fig. 9 for an illustration.

4.3 Conclusions

In this paper, we studied the discrete Gabor frames for finite signals from the need of sparse image modeling As shown in the experiments, compared to the existing wavelet frames often seen in many sparsity-based image recovery methods, the discrete Gabor frames proposed in this paper have their advantages on orientation selectivities and on the flexibilities of modeling both image edges and local textures. In future, we would like to investigate other construction schemes of discrete Gabor tight frames for further performance improvement in image recovery.

References

1. Bölcskei, H., Hlawatsch, F.: Discrete Zak transforms, polyphase transforms, and applications. IEEE Trans. Signal Process. **45**(4), 851–867 (1997) 5, 9
2. Cai, J., Chan, R., Shen, Z.: A framelet-based image inpainting algorithm. Appl. Comput. Harmon. Anal. **24**(2), 131–149 (2008) 5
3. Cai, J., Chan, R., Shen, Z.: Simultaneous cartoon and texture inpainting. Inverse Probl. Imag. **4**(3), 379–395 (2010) 2
4. Cai, J., Don, B., Shen, Z., Osher, S.: Image restoration: total variation ; wavelet frames; and beyond. J. Amer. Math. Soc. **25**(4), 1033–1089 (2012) 5
5. Cai, J., Ji, H., Liu, C., Shen, Z.: Framelet based blind image deblurring from a single image. IEEE Trans. Image Process. **21**(2), 562–572 (2012) 5
6. Cai, J., Osher, S., Shen, Z.: Split Bregman methods and frame based image restoration. Multiscale model. Simul. **8**(2), 337–369 (2009) 5, 6, 14
7. Candes, E., Donoho, D.L.: New tight frames of curvelets and optimal representations of objects with piecewise-C^2 singularities. Comm. Pure Appl. Math. **57**, 219–266 (2002) 1
8. Christensen, O.: An introduction to frames and Riesz bases. Birkhäuser Boston (2002) 4
9. Christensen, O.: Pairs of dual Gabor frame generators with compact support and desired frequency localization. Appl. Comput. Harmon. Anal. **20**(3), 403–410 (2006) 5
10. Coifman, R., Donoho, D.: Translation-invariant de-noising. In: Wavelet and Statistics, *Springer Lecture Notes in Statistics*, vol. 103, pp. 125–150. Springer-Verlag. (1994) 1, 5
11. Cvetkovic, Z., Vetterli, M.: Tight Weyl-Heisenberg frame in $\ell^2(Z)$. IEEE Trans. Signal Process. **46**(5), 1256–1260 (1998) 4, 5, 9
12. Daubechies, I.: Ten Lectures on Wavelets. SIAM (1992) 1, 4, 9
13. Daubechies, I., Han, B., Ron, A., Shen, Z.: Framelets: MRA-based constructions of wavelet frames. Appl. Comput. Harmon. Anal. **14**, 1–46 (2003) 1, 14
14. Daugmann, J.G.: Two-dimensional spectral analysis of cortical receptive field profile. Vision Res. **20**, 847–856 (1980) 2
15. De Boor, C.: B (asic)-spline basics. Mathematics Research Center, University of Wisconsin-Madison (1986) 9
16. Elad, M., Milanfar, P., Rubinstein, R.: Analysis versus synthesis in signal priors. Inverse Probl. **23**(3) (2007) 5
17. Elad, M., Starck, J.L., Querre, P., Donoho, D.L.: Simultaneous cartoon and texture image inpainting using morphological component analysis (mca). Appl. Comput. Harmon. Anal. **19**(3), 340–358 (2005) 5
18. Fan, Z., Heinecke, A., Shen, Z.: Duality for frames. J. Fourier Anal. Appl. **22**(1), 71–136 (2016) 4, 6
19. Fan, Z., Ji, H., Shen, Z.: Dual gramian analysis: duality principle and unitary extension principle. Math. Comp. **85**(297), 239–270 (2016) 4, 6
20. Feichtinger, H.G., Kozek, W., Luef, F.: Gabor analysis over finite Abelian groups. Appl. Comput. Harmon. Anal. **26**(2), 230–248 (2009) 4
21. Gabor, D.: Theory of communication. J. IEE **93**(26), 429–457 (1946) 4
22. Guo, K., Labate, D., Lim, W., Wei, G., Wilson, E.: Wavelets with composite dilations. Electr. Res. Ann. AMS **10**, 78–87 (2004) 1
23. Janssen, A.: Duality and biorthogonality for Weyl-Heisenberg frames. J. Fourier Anal. Appl. **1**(4), 403–436 (1994) 4
24. Janssen, A.: From continuous to discrete Weyl-Heisenberg frames through sampling. J. Fourier Anal. Appl. **3**(5), 583–596 (1997) 5
25. Kutyniok, G., Labate, D.: Construction of regular and irregular shearlet frames. J. Wavelet Theory Appl. **1**, 1–10 (2007) 1
26. Li, S.: Discrete multi-Gabor expansions. IEEE Trans. Inf. Theory **45**(6), 1954–1958 (1999) 5
27. Lim, W.Q.: The discrete shearlet transform: A new directional transform and compactly supported shearlet frames. IEEE Trans. Image Process. **19**(5), 1166–1180 (2010) 15
28. Lopez, J., Han, D.: Discrete Gabor frames in $\ell^2(Z^d)$. Proc. Ame. Thorac. Soc. **141**(11), 3839–3851 (2013) 4
29. Lu, Y., Morris, J.M.: Some results on discrete gabor transforms for finite periodic sequences. IEEE Trans. Signal Process. **46**(6), 1703–1708 (1998) 4
30. Mallat, S., Lepennec, E.: Sparse geometric image representation with bandelets. IEEE Trans. Image Process. **14**, 423–438 (2005) 1
31. Meyer, F.G., Coifman, R.R.: Brushlets: a tool for directional image analysis and image compression. Appl. Comput. Harmon. Anal. **4**(2), 147–187 (1997) 2, 5, 12
32. Morris, J.M., Lu, Y.: Discrete gabor expansion of discrete-time signals in $\ell^2(Z)$ via frame theory. Signal Process. **40**, 155–181 (1994) 4, 5
33. Orr, R.S.: Derivation of the finite discrete Gabor transform by periodization and sampling. Signal Process. **34**(1), 85–97 (1993) 5
34. Qian, S., Chen, D.: Discrete Gabor transform. IEEE Trans. Signal Process. **41**(7), 2429–2438 (1993) 5
35. Qiu, S.: Discrete Gabor transforms: the Gabor-Gram matrix approach. J. Fourier Anal. Appl. **4**(1), 1–17 (1998) 5
36. Ron, A., Shen, Z.: Frames and stable bases for subspaces of $L^2(R^d)$: the duality principle of Weyl-Heisenberg sets. In: Proceedings of the Lanczos Centenary Conference Raleigh, pp. 422–425. SIAM Pub. (1993) 4, 6
37. Ron, A., Shen, Z.: Affine system in $L_2(R^d)$: the analysis of the analysis operator. J. of Func. Anal. **148** (1997) 1, 14
38. Ron, A., Shen, Z.: Weyl-Heisenberg Frames and Riesz Bases in $L^2(R^d)$. Duke Math. J. **89**, 237–282 (1997) 4, 5, 6, 7, 8
39. Selesnick, I.W., Baraniuk, R.G., Kingsbury, N.C.: The dual-tree complex wavelet transform. IEEE Signal Process. Mag. **22**(6), 123–151 (2005) 2, 12, 14
40. Shen, Z.: Wavelet frames and image restorations. Proc. ICM (2010) 5
41. Søndergaard, P.L.: Gabor frames by sampling and periodization. Adv. Comput. Math. **27**(4), 355–373 (2007) 5
42. Starck, J., Candès, E.: The curvelet transform for image denoising. IEEE Trans. Image Process. **11**(6), 670–684 (2002) 5
43. Starck, J., Nguyen, M., Murtagh, F.: Wavelets and curvelets for image deconvolution: a combined approach. Signal Process. **83**(10), 2279–2283 (2003) 5
44. Starck, J.L., Elad, M., Donoho, D.L.: Image decomposition via the combination of sparse representations and a variational approach. IEEE Trans. Image Process. **14**, 1570–1582 (2005) 2
45. Wang, Y., Yang, J., Yin, W., Zhang, Y.: A new alternating minimization algorithm for total variation image reconstruction. SIAM J. Imag. Sci. **1**, 248–272 (2008) 14
46. Wexler, J., Raz, S.: Discrete gabor expansions. Signal Process. **21**(3), 207–220 (1990) 4, 5